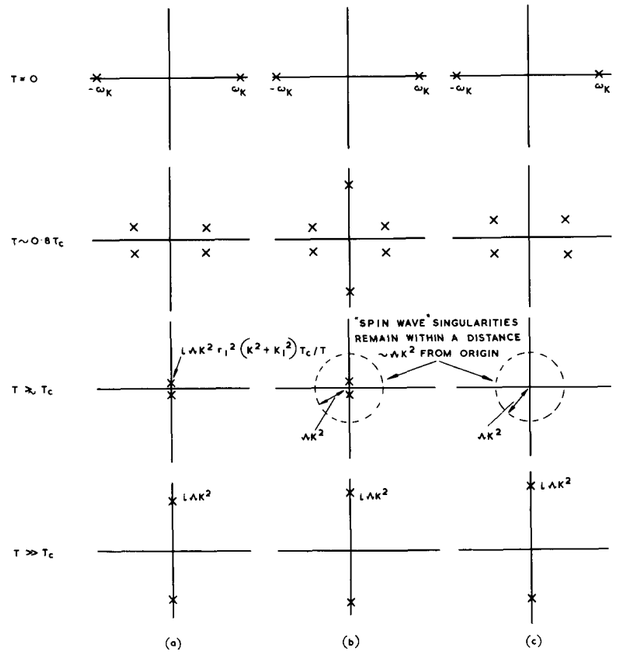

FIGURE 1. *Possible singularities of* $F^{xx}(\mathbf{K}, \omega)$ *in the complex* ω*-plane.*
Figure 1a shows the results of conventional theory. Figure 1b indicates the qualitative nature of the singularities of the analogy to hydrodynamics holds. Figure 1c indicates an alternative possibility in which poles do not collapse to the origin at T_c. In all diagrams the singularities at distances $\sim J/\hbar$ from the origin are ignored.

which are a long distance $\sim J/\hbar$ from the origin are not shown. Figure 1a gives the conventional theory, figure 1b the theory we would expect by analogy to hydrodynamics and figure 1c the theory we might expect if no "diffusive" mode appears below T_c. At the present time we are not able to tell whether possibility, (b) or (c) is correct.

5. Further Experiments

In this section we shall list briefly other experiments which give information on the form of $F^{xx}(\mathbf{K}, \omega)$.

(a) In experiments on Fe_3O_4, Riste [14] observed that spin waves existed above T_c and plotted their lifetime as a function of temperature. His results can be taken as experimental evidence in favor of the existence of spin waves above T_c. Unfortunately his experiments did not cover a wide enough range of scattering surfaces to distinguish between figures 1b and 1c.

(b) Although all the discussion of this paper has concerned ferromagnets we would naturally expect to carry over some results to antiferromagnets. In particular if spin waves exist above T_c in a ferromagnet we would expect them to exist above the Neél temperature of an antiferromagnet. It is therefore worth noting that Murthy et al. [15], have observed spin waves in MnO above the Neél temperature. As we would expect, these spin waves peaks are broad. MnO is an unusual antiferromagnet in that $T_N \sim 120$ °K but $\theta \sim 600$ °K; therefore at the Neél temperature we expect an exceptional amount of short range order to exist. In the presence of this large short range order we would expect the spin waves to be better defined than in the typical antiferromagnet and therefore in figures 1b and 1c the "spin wave" singularities would approximate closer to simple spin wave poles. This is probably why these neutron experiments observed them whereas experiments on other antiferromagnets, for example, Turberfield et al. [16], on MnF_2 do not see distinct spin waves above T_N.

6. Conclusions

The theory of neutron scattering from ferromagnets has been reviewed and it is shown how the experiments give the wavelength dependent susceptibility unambiguously. The experiments show that the conventional theory of the time dependence of the fluctuations near T_c, is incorrect. It is too difficult to construct an alternative theory immediately but to explain the results it is necessary that some remnant of "spin-wave motion" remains above T_c. Two possibilities are described in terms of the singularities of the relaxation function in the complex ω-plane.

7. References

[1] C. Domb and M. F. Sykes, Phys. Rev. **128,** 168, (1962).
[2] J. Gammel, W. Marshall and L. Morgan, Proc. Roy. Soc. **275,** 257 (1963).
[3] M. E. Fisher and M. F. Sykes, Physica **28,** 939 (1962).
[4] M. F. Sykes and M. E. Fisher, Physica **28,** 919 (1962).
[5] H. Mori and K. Kawasaki, Prog. Theor. Phys. **25,** 723 (1962).
[6] L. Passell, K. Blinowshi, P. Nielsen and T. Brun, Proc. International Conference on Magnetism.[1]
[7] R. Elliott and W. Marshall, Rev. Mod. Phys. **30,** 75 (1958).
[8] P. G. de Gennes, J. Phys. Chem. Solids **4,** 223 (1958).
[9] L. Van Hove, Phys. Rev. **95,** 1374 (1954).
[10] P. G. de Gennes and J. Villain, J. Phys. Chem. Solids **13,** 10 (1960).
[11] B. Jacrot, J. Kostantinovic, G. Perette and D. Cribier.[2]
[12] L. D. Landau and E. M. Lifshitz, Fluid Mechanics, Pergamon Press.
[13] W. Marshall, Lectures on Critical Phenomena, A.E.R.E.-L. 144 (1964).
[14] T. Riste, Journal Phys. Soc. Japan **17,** Supplement Bill, 60 (1962). Proc. of International Conference on Magnetism and Crystallography.
[15] N. S. Satya Murthy, G. Venkataraman, K. Usha Denig, B. A. Dasannacharya and P. K. Iyengar, Symposium on Inelastic Neutron Scattering, Bombay, 1964.
[16] K. C. Turberfield, A. Okazaki, and R. W. H. Stevenson, Proc. Phys. Soc. **85,** 743 (1965).

[1] Nottingham 1964, 99.
[2] Symposium on Inelastic Scattering of Neutrons in Solids and Liquids, Chalk River, 1962.

Critical Magnetic Scattering of Neutrons in Iron

L. Passell

Brookhaven National Laboratory, Upton, N.Y.

Abstract

Measurements of the angular and energy distributions of 4.28 Å neutrons scattered at small angles from iron at temperatures above the Curie temperature are described. The results are interpreted in terms of Van Hove's theory of critical magnetic scattering and yield information on the range of spin correlations and the dynamics of the spin ordering process. For the dimensionless parameter, $2m\Lambda/\hbar$, which describes the time dependence of the spin fluctuations, we obtain the value 11.0 ± 0.6 at $T - T_c = 2$ and 18 °C. The zero field magnetic susceptibility, as determined by the parameters κ_1 and r_1 (which represent the range and strength respectively of the spin correlations), is found to vary as $(T - T_c)^{-1.30 \pm 0.04}$. Near the Curie temperature there was sufficient intensity to measure the ratio of the coefficients of the K^4 and K^2 terms of the angular distribution. The value of this ratio, 29 Å^2, is related to the existence of long range couplings within the spin system. Details of certain recent modifications of the theory of critical systems are discussed and compared with the experimental results.

This work is described in detail in a paper by L. Passell, K. Blinowski, T. Brun and P. Nielsen, Phys. Rev. **139A,** 1886 (1965).

Critical Neutron Scattering From Beta-Brass

O. W. Dietrich and J. Als-Nielsen

Research Establishment Risö, Roskilde, Denmark

Introduction

Beta-brass, which is an approx. 50 percent to 50 percent alloy of Cu and Zn, forms at low temperatures an ordered B.C.C. lattice. A B.C.C. lattice can be thought of as composed of two S.C. lattices—so-called superlattices, denoted respectively A and B—displaced half a cube diagonal with respect to each other. Perfect order means that all Cu atoms are at A sites, all Zn atoms at B sites. The order gradually decreases with increasing temperature; at the critical temperature T_c ($T_c \simeq 468$ °C) the average occupation of say an A site is entirely random, i.e., the long range order (abbr. LRO) has disappeared. Above T_c, however, local order still exists: If a certain A site is occupied by say a Zn atom there will be an excess probability over randomness that the nearest site—a B site—is occupied by a Cu atom and so on. This local order or short range order is described by a pair correlation function (abbr. pcf.)

In a diffraction experiment the LRO will give rise to narrow diffraction peaks (Bragg scattering peaks), whereas the SRO will give rise to broader and less intense peaks (critical scattering) provided that the radiation is scattered sufficiently different from a Cu atom and a Zn atom. This criterion make neutrons more suitable than x rays in case of β-brass. Walker and Keating have previously reported on a neutron scattering experiment from a β-brass crystal [1], which was furthermore enriched with Cu^{65} to enhance the difference in scattering amplitudes. Due to rapid Zn-evaporation from their crystal, it is however not possible to draw detailed quantitative conclusions from this experiment. From our present experiment, where a β-brass single crystal with normal isotopic abundance was used, the following can be deduced:

(1) The temperature dependence of LRO in the close vicinity of T_c,

(2) the absolute value and the temperature dependence of the SRO correlation range, and

(3) some conclusions concerning the shape of the pair correlation function.

Cross Section

The changes in occupation of lattice sites are believed to be so slow that a static approximation is rigidly valid in deriving the relevant cross section. The cross section for a scattering vector $\boldsymbol{\kappa}$ close to a superlattice point $\boldsymbol{\tau}$ in the reciprocal space is

$$\frac{d\sigma}{d\Omega} \sim e^{-2W}\left(\frac{a-b}{2}\right)^2\left[\mathrm{LRO}^2\boldsymbol{\delta}(\boldsymbol{\kappa}-\boldsymbol{\tau}) + \Sigma_{\mathbf{R}}\,\mathrm{pcf}\,(\mathbf{R})e^{-i\boldsymbol{\kappa}\cdot\mathbf{R}}\right] \quad (1)$$

a and b denote respectively the scattering amplitudes for Cu and Zn nuclei, $\mathbf{R}$ is a direct lattice vector and the Debye-Waller factor e^{-2W} accounts for the influence of the thermal vibrations on elastic scattering.

For $T < T_c$ the temperature dependence of $(\mathrm{LRO})^2$ is deduced from the Bragg peak intensities. For $T > T_c$ this kind of scattering disappears and only critical scattering remains. It will later be shown that the Ornstein-Zernike pcf $\sim \frac{1}{r_1^2}\, e^{-\kappa_1 R}/R$ fits the critical scattering data excellently, and with this shape of the pcf the critical scattering cross section becomes:

$$\left(\frac{d\sigma}{d\Omega}\right)\mathrm{crit} \sim \frac{1}{r_1^2}\cdot\frac{1}{|\boldsymbol{\kappa}-\boldsymbol{\tau}|^2+\kappa_1^2} \quad (2)$$

κ_1 is called the inverse correlation range, r_1 the strength parameter.

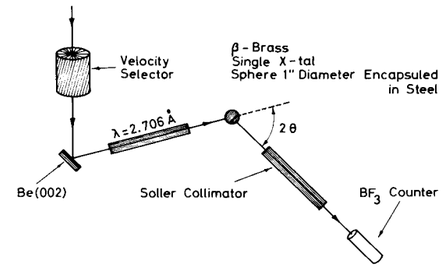

FIGURE 1. *Experimental setup in the (1, 0, 0) reflection.*
The angle between vertex and (0, 0, 1) is approx. 12°, whereby the occurrence of multiple scattering is prohibited.

The Experimental Setup

Monochromatic neutrons were extracted from the polyenergetic reactor beam by (0,0,2)—Bragg reflection in a Be single crystal (mosaic spread 5′ s.d.). Higher order neutrons were filtered out by means of a mechanical velocity selector (see fig. 1). A rather long wavelength of 2.70 Å was chosen to safely avoid parasitic multiple Bragg reflections in the β-brass single crystal, which in the (1,0,0) reflection was oriented with (0,0,1) approx. 12° from vertex. Also the instrumental resolution could be made quite narrow at this wavelength, which is essential for the interpretation of the critical scattering as shown below. The reactor beam was only collimated by the beam tube dimensions, the monochromatic beam was cylindrically collimated (30 mm diam per m) and the scattered beam was horizontally collimated by Soller slits (3.5 mm per m). The monochromatic beam intensity was $2.5 \cdot 10^5$ neutrons/sec. The counting time was mastered from a preset count on a monochromatic beam monitor (abbr. BMc in figures).

The spherical crystal (1 in. diam) was tightly encapsuled in a thin stainless steel container to avoid Zn evaporation. A 5 percent variation of the Zn content changes T_c 14 °C, [2] but in the six-months duration of the experiment T_c remained constant within a few tenth's of a degree. The crystal was mounted in an oven of sufficiently wide diameter so neutrons scattered from irradiated parts of the walls of the heating coil could not possibly hit the BF_3-detector. The crystal table could be turned around a horizontal and a vertical axis; the latter could also be coupled in the ratio 1:2 to the spectrometer arm. Two different scan types through a superlattice reflection in reciprocal space is sketched in figure 2.

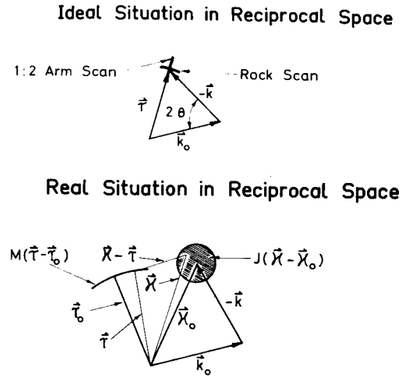

FIGURE 2. *Upper part: Wavevectors in reciprocal space corresponding to figure 1 (idealized resolution).*
Lower part: Definitions of distribution function with finite resolution.
The contour of $J(\boldsymbol{\kappa}-\boldsymbol{\kappa}_0)$ indicates f.i. a horizontal cut in the surface of half widths.

Instrumental Resolution

Due to instrumental resolution the endpoint of the scattering vector $\boldsymbol{\kappa}$ is smeared, which is indicated by the distribution function $J_{\kappa_0}(\boldsymbol{\kappa})$. In the limited region in reciprocal space, where $J_{\kappa_0}(\boldsymbol{\kappa})$ will be used in the calculations below it is assumed that J is only dependent on the difference $\boldsymbol{\kappa}-\boldsymbol{\kappa}_0$, i.e., $J_{\kappa_0}(\boldsymbol{\kappa}) = J(\boldsymbol{\kappa}-\boldsymbol{\kappa}_0)$. Also the endpoint of the $\boldsymbol{\tau}$-vector is smeared due to the mosaic spread, indicated by the distribution function $M(\boldsymbol{\tau}-\boldsymbol{\tau}_0)$(see fig. 2). The intensity $I(\boldsymbol{\kappa}_0, \boldsymbol{\tau}_0)$ with the spectrometer and crystal set at the average values $\boldsymbol{\kappa}_0$ and $\boldsymbol{\tau}_0$ of the scattering vector and $\boldsymbol{\tau}$-vector respectively is found as the 6-dimensional convolution integral:

$$I(\boldsymbol{\kappa}_0, \boldsymbol{\tau}_0) = \int\int J(\boldsymbol{\kappa}-\boldsymbol{\kappa}_0)\cdot M(\boldsymbol{\tau}-\boldsymbol{\tau}_0) \cdot\sigma(\boldsymbol{\kappa}, \boldsymbol{\tau})\, d\boldsymbol{\kappa} d\boldsymbol{\tau}, \quad (3)$$

where the cross section $\frac{d\sigma}{d\Omega}(\boldsymbol{\kappa}, \boldsymbol{\tau})$ has been abbreviated to $\sigma(\boldsymbol{\kappa}, \boldsymbol{\tau})$.

For Bragg scattering $\sigma(\kappa, \tau) = \delta(\kappa - \tau)$ and

$$I_{\text{Bragg}}(\kappa_0 - \tau_0) = \int\int J(\kappa - \kappa_0) M(\tau - \tau_0) \delta(\kappa - \tau) d\kappa d\tau. \quad (4)$$

For critical scattering $\sigma(\kappa, \tau) = \sigma(\kappa - \tau) = \int \sigma(\epsilon) \delta(\kappa - \tau - \epsilon) d\epsilon$

and

$$I_{\text{crit}}(\kappa_0 - \tau_0) = \int \sigma(\epsilon) d\epsilon \int\int J(\kappa - \kappa_0) M(\tau - \tau_0) \cdot \delta(\kappa - \tau - \epsilon) d\kappa d\tau$$

$$= \int \sigma(\epsilon) d\epsilon \int\int J(\kappa^* - (\kappa_0 - \epsilon)) M(\tau - \tau_0) \cdot \delta(\kappa^* - \tau) d\kappa^* d\tau$$

$$I_{\text{crit}}(\kappa_0 - \tau_0) = \int I_{\text{Bragg}}(\kappa_0 - \epsilon - \tau_0) \sigma(\epsilon) d\epsilon \quad (5)$$

The measured critical scattering is thus the 3-dimensional convolution integral of a measurable function $I_{\text{Bragg}}(\kappa_0 - \tau_0)$ and the cross section σ, and an exact convolution can be performed without any assumptions of the shape of the distribution functions $J(\kappa - \kappa_0)$ and $M(\tau - \tau_0)$, apart from the already mentioned approximation $J_{\kappa_0}(\kappa) \simeq J(\kappa - \kappa_0)$.

Analysis of Critical Diffraction Peaks

In practice, the unfolding calculation was performed in the following way with the aid of a digital computer:

Three mutual perpendicular scans through the Bragg peak were measured below T_c and approximated by three normalized Gaussians. The product of these was used as $I_{\text{Bragg}}(\kappa_0 - \tau_0)$. In f.i. a rock scan measurement the computer calculated the ratio between $\sigma(\kappa_0, \tau_0)$ from (2) and $I(\kappa_0, \tau_0)$ from (5) for different directions of τ_0 and for a certain value of κ_1. For this value of κ_1 the sum of weighted, squared deviations between $I(\kappa_0, \tau_0)$ and the measured intensities was calculated, and by iteration in κ_1-values this sum was finally minimized.

An example is demonstrated in figure 3, where a scan perpendicular to (1, 0, 0) was measured 4.4 °C above T_c. The circular points are measured intensities as function of crystal setting. The narrow curve is the corresponding normalized Bragg reflection peak, measured below T_c, and the dashed curve is the Lorentzian (2) for the best κ_1-value. These curves are drawn upon a constant background, which was measured at several points far from the superlattic point (1, 0, 0). A scan at a high temperature (70° above T_c) showed the same constant background, when corrected for the remaining small amount of critical scattering. This justifies to some extent a constant background subtraction, which was used throughout the analysis of all critical data.

It is seen that the Ornstein-Zernike pair correlation function fits the data excellently. The scatter of measured points around the folded Lorentzian (solid line) is random and in statistical agreement with the uncertainties on the count rates.

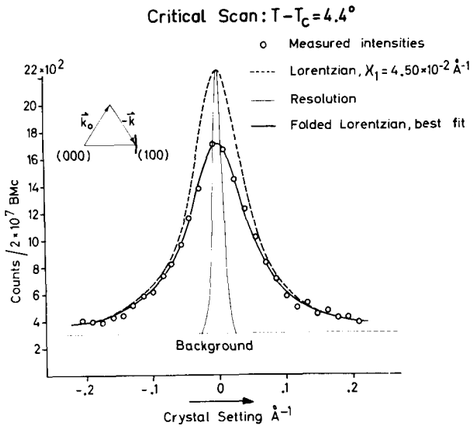

FIGURE 3. *A rock-scan through (1, 0, 0) 4.4° above* T_c. The excellent fit of an Ornstein-Zernike correlation function is apparent.

Best Fit for Different Correlation Functions

Pair Correlation Function			$T-T_c$ 2.0°	4.4°	5.7°	12.1°
Ornstein Zernike	$\frac{e^{-X_1 R}}{R}$	X_1	2.38×10^{-2}	4.54×10^{-2}	5.12×10^{-2}	6.82×10^{-2}
Fisher	$\frac{e^{-X_1 R}}{R^{1+\eta}}$	X_1	2.38×10^{-2}	4.54×10^{-2}	5.12×10^{-2}	6.82×10^{-2}
		η	0.0000	0.0000	0.0000	0.0000
Hart	$\frac{e^{-X_1 R}}{R}\left[1-e^{-(1-X_1)R}\right]$	X_1	2.38×10^{-2}	4.54×10^{-2}	5.12×10^{-2}	6.82×10^{-2}
		η	1.00×10^{6}	1.08×10^{6}	2.97×10^{5}	2.32×10^{6}

Temperature Dependence of LRO and SRO

Theoretically (LRO), which is proportional to the Bragg peak intensity, is proportional to $(T_c - T)^{2\beta}$ with $\beta \simeq 5/16 = 0.3125$ for the Ising Model [5].

Figure 4 shows the peak intensity from the (1,1,1) reflection as function of the temperature from 10° below the critical temperature to a little above this point. When the intensities are plotted as function of $\Delta T \equiv T_c - T$ in a double log plot, it is seen that a power law is valid near T_c and that $\beta \simeq 0.325$.

The intersection of the long-range order curve with the abscissa gives the thermocouple voltage when the crystal is in the critical state. The temperature dependence of all the parameters to be discussed is expressed by the temperature difference ΔT and this is measured as the corresponding difference in thermocouple voltage multiplied with the scaling factor 0.103 °K/μV. The uncertainty of the intersection contributes the main part of the uncertainty of 0.1 °K on ΔT.

A possible temperature gradient can be found by measuring similar curves with reduced beam hitting different parts of the crystal. The currents in the heating coils in the oven were adjusted until all curves intersected the abscissa at the same thermocouple voltage, and it was then concluded that temperature gradients could be neglected.

Figure 5 shows similar curves for the (1,0,0) reflection. β is here found to be 0.27 which differs significantly from the value 0.325 obtained from the (1, 1, 1) reflection. This might be due to a different degree of extinction in the two cases. The extinction correction will be relatively larger for big values of ΔT than for small values, since the cross section and thereby the beam attenuation through the crystal increases with increasing values of ΔT. The extinction correction will therefore qualitatively have the effect of increasing the slope of the line in the double log plot. At present we have not investigated this problem in detail, and the figures show uncorrected Bragg peak intensities.

The tail of the curve for temperatures above the critical point is the peak intensity of the critical scattering, and the difference in order of magnitude from the Bragg peak intensity should be noted.

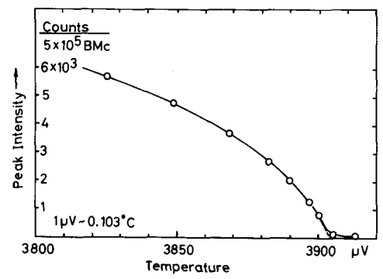

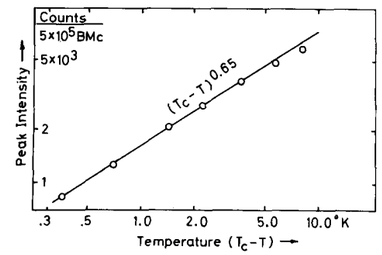

FIGURE 4. *Bragg peak intensity versus temperature for the (1, 1, 1) reflection.*

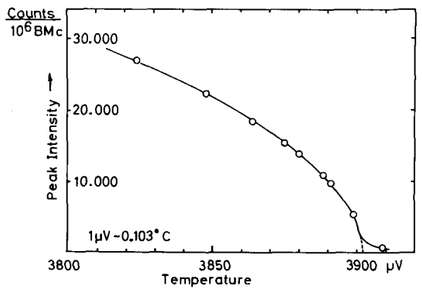

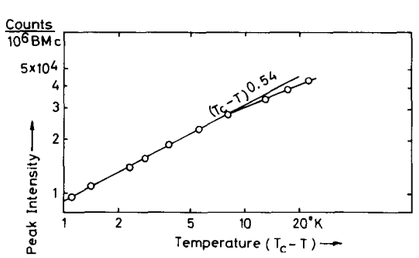

FIGURE 5. *Bragg peak intensity versus temperature for the (1, 0, 0,) reflection.*

209-493 O-66 11

Also the temperature dependence of the SRO has been calculated in the Ising Model. For a ferromagnet it has been found that the susceptibility χ obeys a power law being proportional to $\left(\frac{T-T_c}{T}\right)^{\gamma}$ with γ equal to 1.25 [5]. It is a well known fact that the susceptibility χ is related to the pair correlation function through ($\chi \propto \Sigma_R$ pcf (R)).

On the other hand the peak intensity I_0 for $T > T_c$ is also proportional to this sum as seen from the cross section formula (1). Recalling the close analogy of the order-disorder transition in alloys and magnetic materials, it is therefore expected that $I_0 \propto \left(\frac{T-T_c}{T}\right)^{-\gamma}$. γ can therefore be determined from the measured temperature dependence of the peak intensity, *independently* of any shape that the pair correlation function might have, provided of course that the resolution correction is correct.

Figure 6 shows the peak intensities of critical scattering from the (1, 0, 0) and from the (1, 1, 1) reflections for temperatures up to about 35° above T_c. The intensities are corrected for reduction due to resolution and the curves shown in the lower part of the figure show the corrections. The peak value reduction amounts to as much as a factor of 2 at the lowest temperatures and since the corrected intensities for both reflections obey the same power law, this gives confidence in the calculations on resolution corrections.

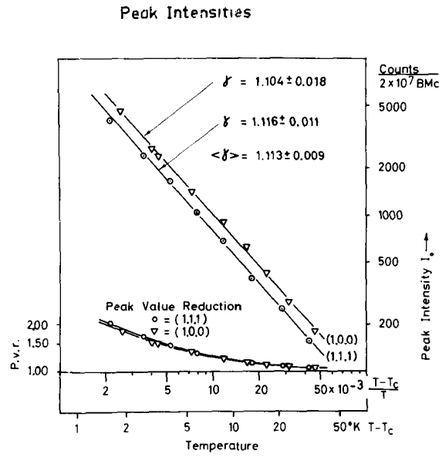

FIGURE 6. *Critical peak intensities, corrected for resolution reduction, for (1, 0, 0) and (1, 1, 1) reflections.*

The difference between peak intensities for the (1, 0, 0) and the (1, 1, 1) reflections is due to different Debye-Waller factors. The measured ratio is seen to be 1.28 and, using Chipmann's data for the Debye temperature around 750 °K [6], the ratio of the Debye-Waller factors is 1.32.

The weighted average value of the power γ is 1.11 ± 0.01, which should be compared with the theoretical value of 1.25.

Figure 7 shows the values of κ_1 obtained at different temperatures in different scan types through different superlattice points in the reciprocal lattice. It is worthwhile to note the consistency of the results. Each point represents one diffraction peak, which takes, on an average, 48 hrs of measuring time.

For comparison with theory, the value of κ_1 at 75° above T_c calculated from the theory of Elliott and Marshall is also shown.

The peak intensity I_0 is with the Ornstein-Zernike pcf proportional to $(r_1 \cdot \kappa_1)^{-2}$.

r_1 is theoretically expected to decrease slightly with increasing temperature [7]. This implies that twice the slope of the least square fitted line to the κ_1-values is an upper limit of the parameter γ already discussed. It is concluded therefore that γ is less than 1.18 ± 0.02, in consistency with the value found from the peak value runs.

On the other hand, the measured values of κ_1 together with the experimental result that $(r_1 \cdot \kappa_1)^{-2} \propto \left(\frac{T-T_c}{T}\right)^{-1.11}$, can be used to deduce the temperature dependence of r_1. In a linear approximation with $r_1^2 = r_{1c}^2\left(1-\alpha\frac{\Delta T}{T}\right)$, it was found that α was equal to 3.6 ± 1.2. which is compared with the temperature dependence of r_1 given by Elliott and Marshall [7], who found that $\alpha \simeq 1.2$.

FIGURE 7. *Inverse correlation ranges κ_1 versus temperature.*
Each point represents the result of a scan as shown in figure 3.

After completion of these measurements it was concluded that the most accurate information could be obtained from rock-scans through the (1, 0, 0) reflection. A series of such scans were therefore measured, but the inverse correlation ranges were now found to be 20 percent lower than the previous data over the entire temperature region as shown on figure 8.

The (1, 1, 1) reflection data, which was obtained at the end of the previous run, tends toward the data of the latest (1, 0, 0) reflection run. The critical temperature, as well as the Bragg peak intensities, were still exactly reproducible. Also the temperature dependences of κ_1 and I_0 as well as $I_0(\kappa_1)$ are in agreement with the previous data. It must therefore be concluded that some properties of the crystal have changed during the long period at elevated temperatures, but we are unable to give any detailed explanation of the change. Future experiments on other β-brass crystals might shed light on the problem.

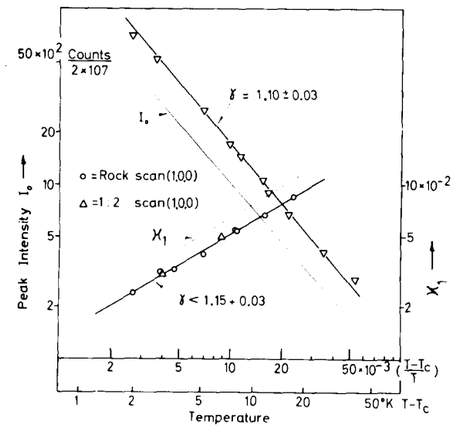

FIGURE 8. *Later results of critical scattering around the (1, 0, 0) reflection.*
These results are not consistent with the results in figure 6 and figure 7. Note, however, that T_c, β, γ, and $I_0(\kappa_1)$ are the same.

Conclusion

The following conclusions can be drawn from the present experiment:

(1) The Ornstein-Zernike correlation function is in excellent agreement with the data. A complete Fourier analysis to obtain all SRO parameters is not possible due to the very limited regions of the reciprocal space where the critical scattering is sufficiently intense for experimental access.

(2) The absolute value of the short range order correlation range is roughly in agreement with theory, but could possibly be an individual property of a given crystal.

(3) The temperature dependence of LRO is not in contradiction to the latest Ising model results, but definitely outrules the results of older theories $\left(\text{f.i. Bethe-Peierls theory, } \beta = \frac{1}{2}\right)$.

(4) The temperature dependence of SRO is in slight but definite disagreement with the Ising model in the nearest-neighbor interaction approximation.

Note added in proof. Later measurements have indicated that the β-brass crystal contains a few percentages of γ-phase. Recent measurements on a pure β-brass crystal gave an exponent in the temperature law for the susceptibility of $\gamma = 1.25 \pm .02$.

References

[1] Walker, C. B., and Keating, D. T., Phys. Rev. **130,** 1726 (1963).
[2] Hansen, M., Constitution of Binary Alloys (McGraw-Hill Book Co., New York., N.Y., 1958).
[3] Fisher, M. E., Physica **28,** 172 (1962).
[4] Hart, E. W., J. Chem. Phys. **34,** 1471 (1961).
[5] Essam, I. M., and Fisher, M. E., J. Chem. Phys. **38,** 802 (1963).
[6] Chipman, D. R., MRL Report No. 67, Watertown Arsenal, Massachusetts (1959).
[7] Elliott, R. I., and Marshall, W., Rev. Mod. Phys. **30,** 1 (1958).